Chapter

Two-Dimensional Group-10 Noble-Transition-Metal Dichalcogenides Photodetector

Haoran Mu, Jian Yuan and Shenghuang Lin

Abstract

2D Transition-Metal Dichalcogenides (TMDs) have been widely considered as a promising material for future optoelectronics due to the strong light-matter interaction, fantastic electronic properties and environmental stability. However, the relatively large bandgap and low mobility of conventional TMDs (such as MoS_2 and WS_2) limit their applications in infra optoelectronics and high-speed photodetection. In this chapter, we introduce a new type of group-10 noble TMDs (NTMDs), which exhibit outstanding properties such as unique structural phase, widely tunable energy gap and high mobility. Till now, various NTMDs-based photodetectors have been realized with ultrabroad detection waveband (200 nm to 10.6 μm), fast response time, high responsivity and detectivity, and polarization sensitivity. NTMDs have been excellent potential candidates for next-generation photodetection devices with high-performance, wafer-scalability and flexibility.

Keywords: noble-transition-metal dichalcogenides, 2D materials, photodetectors, optoelectronics, van der Waals

1. Introduction

Photodetectors, which can capture, identify and visualize the optical signals, have been indispensable devices in modern integrated electronics and communication technology [1–5]. Nowadays, various photosensitive materials have been investigated as the functional materials in photodetectors. For example, gallium nitride (GaN) is commercially for ultraviolet light detection (UV, <400 nm), Si for visible–near-infra (NIR, 400–1100 nm), InGaAs for NIR–mid-IR (MIR, 1–5 μm), and HgCdTe for MIR–far-IR detection (FIR, >5 μm) [2]. However, the ultra-miniaturization and integration of photodetectors with multi-materials are challenging, which require complex nanomanufacturing process and exorbitant production costs. In addition, there are some inherent disadvantages. For example, poor flexibility is a common problem in these conventional semiconductor materials, which restricts their application potential in flexible and wearable electronics. Some specific materials (*e.g.,* HgCdTe) are environment toxic and cannot operated at room temperature [1]. The development trend for high-performance detection and different application scenarios prompts scientists to continue to pursue new materials with novel physical properties.

Two-dimensional (2D) materials have attracted tremendous attention in the past few decades [6–12]. Among them, 2D Transition-Metal Dichalcogenides (TMDs) are considered to be promising for next-generation optoelectronics due to the strong light-matter interaction, weak interlayer van der Waals (vdW) interaction, flexible characteristics and the ease of integration with current silicon-based optical electronics [13–17]. Group-10 noble TMDs (NTMDs) are outstanding representatives in the TMDs family [18–20]. The reintroduced new materials are generalized formulated by Group-10 noble elements (Pt, Pd, and so on.) and chalcogens (S, Se, or Te). Unlike traditional TMDs, the d-electrons in NTMDs are fully occupied their d-orbitals resulting in the highly hybridized P_z orbits and strong interlayer interactions [21, 22]. Therefore, NTMDs exhibit relatively small and widely tunable bandgaps compared with traditional TMDs (such as MoS_2 and WS_2). For example, PtS_2 shows a layer-dependent bandgap from 1.6 to 0.25 eV [21], while $PtSe_2$ changes from a typical semiconductor state (1.2 eV in 1 L $PtSe_2$) to semi-metal state when the thickness increases to over 5 layers [23]. Combining with the high mobility (>1000 $cm^2V^{-1}S^{-1}$, larger than most other TMDs and comparable for that of BP) and environmental stability, NTMDs has great potential in photodetectors applications [21, 23–25]. Moreover, the unique puckered pentagonal structure of PdS_2 and $PdSe_2$ inherently provides them with anisotropic properties [26–28] and may promote the development of polarized photodetectors.

In this chapter, we first discuss the structural, electronic and optical properties of NTMDs. Then we focus on the NTMDs based photodetectors. Wafer-scale NTMDs films with high-quality and large-scale monocrystalline NTMDs nanosheets have been fabricated, which are appropriate for optoelectronic applications. NTMDs and their heterostructure based photodetectors show many advantages such as high-performance, ultrawide spectra detection, long-term environment stability, and anisotropic characteristics. NTMDs have great potential for large-scale imaging and flexible devices, which could be the next-generation optoelectronic core materials.

2. Structural and electronic properties of 2D NTMDs

The atomic coordination of monolayer TMD usually is either trigonal prismatic phase (2H or D_{3h}) or octahedral phase (1 T or D_{3d}), as shown in schematics in **Figure 1a** and **b** [22, 29, 30]. In 2H phase, the d orbitals in transition metal centers split into three degenerated d orbitals (d_{z^2}, $d_{x^2-y^2,xy}$ and $d_{xz,yz}$) and there is usually an energy bandgap (~1 eV in TMDs) between the first two degenerated d orbitals. While in 1 T phase, the centers of transition metal have two degenerated d orbitals (d_{z^2,x^2-y^2} and $d_{xz,yz,xy}$) [22, 29, 30]. Therefore, the thermodynamically favored phase is highly influenced by d electrons count in the transition metals. For NTMDs, the noble metal atoms have abundant d electronics and the d^2sp^3 hybridization is preferred, which lead to the full-filled d-bands. Most NTMDs have thermo-dynamically favored 1 T phase, such as $PtSe_2$, PtS_2, $PtTe_2$ and $PdTe_2$ (See **Figure 1c**) [31]. The strong interlayer hybridization of adjacent chalcogen atoms makes the widely tunable electronic energy band structure with the layer numbers. Here we use PtS_2 and $PtSe_2$ as examples. Both of them are 1 T favored phase, where the bandgap is about 1.17 and 1.6 eV in monolayer $PtSe_2$ and PtS_2, respectively (**Figure 1e** and **f**) [21]. With the increase of stacked layers, the interlayer hybridization would be stronger, with lead to the rapidly decrease of energy gap. According to theoretical calculations, the energy gap in bi-layer $PtSe_2$ is only 0.3 eV, while the stacked layered increase beyond 4 layers, the energy level of valence band

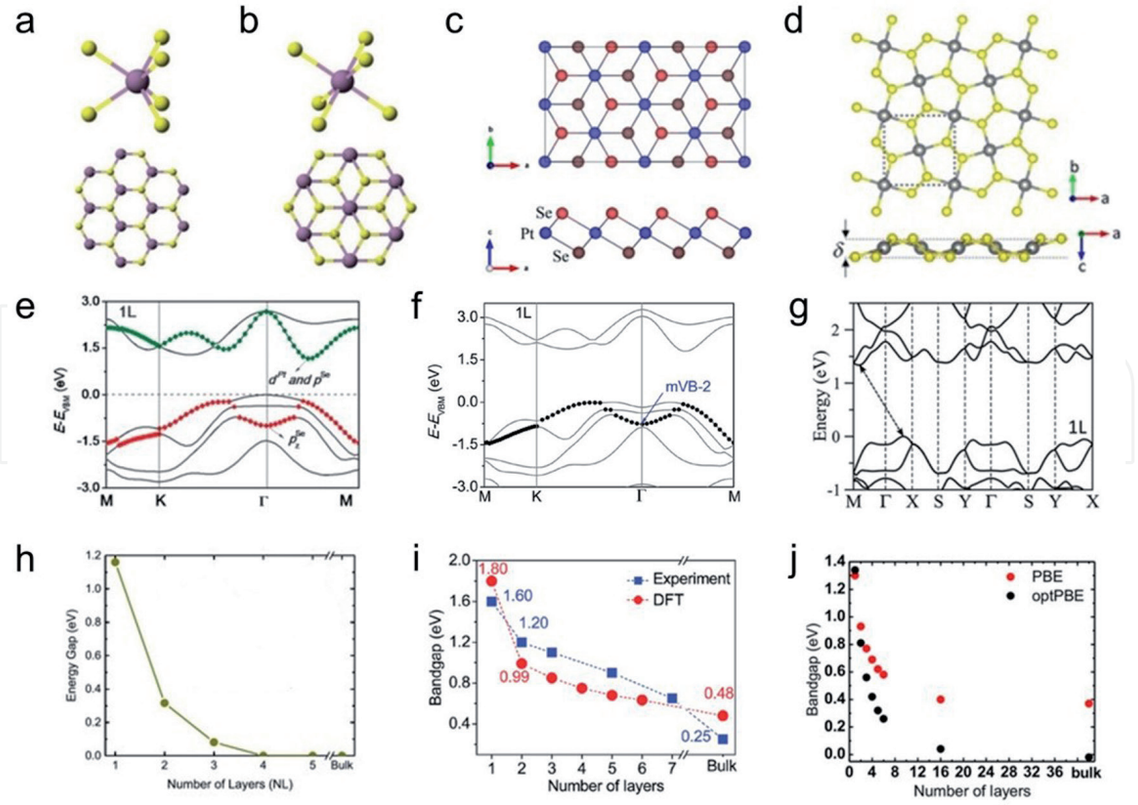

Figure 1.
Crystal and electronic structure of NTMDs. (a) and (b) schematic images of 2H and 1 T lattice phase in TMDs, reproduced with permission [30]. (c) Thermodynamically favored 1 T-phase structural schematic of $PtSe_2$, reproduced with permission [31]. (d) Puckered pentagonal structure of $PdSe_2$, reproduced with permission [26]. (e) Energy band structure of monolayer $PtSe_2$, reproduced with permission [23]. (f) Energy band structure of monolayer PtS_2, where bands mVB-2 were highlighted spanning the Brillouin zone by black dots. (g) Calculated electronic band structures of monolayer $PdSe_2$ by the optPBE method. (h)-(j) evolution of energy bandgap as a function of the number of layers of $PtSe_2$(h), PtS_2(i) and $PdSe_2$(j). (h) Is reproduced with permission [32]. (f) and (i) are reproduced with permission [21]. (g) and (j) are reproduced with permission [26].

maximum (VBM) will exceed that of conduction band minimum (CBM) and $PtSe_2$ undergoes a transition from semiconductor to metallic state (**Figure 1h**) [32]. Similarly, as shown in **Figure 1i**, the energy bandgap in bulk PtS_2 decreases to 0.25 eV from 1.6 eV.

Apart from conventional TMDs materials with hexagonal structures, PdS_2 and $PdSe_2$ consist of pentagonal rings with the puckered vertical conformation (**Figure 1d**) [26]. In each layer, a Pd atom binds to four chalcogen atoms other than six chalcogen atoms, while every two neighbor chalcogen atoms bind each other with a covalent bond. The unique pentagonal structure not only provides the materials with anisotropic properties, but also can realize the transition of topological quantum phase and the spin-orbit coupling enhancement. In 2017, Akinola O., et al. experimentally and theoretically prove that monolayer $PtSe_2$ has 1.3 eV indirect band gap and semi-metal state in the bulk (**Figure 1g** and **j**) [26].

3. Optical properties of 2D NTMDs

The widely tunable electronic energy gap of NTMDs make them layer-dependent optical absorption [32]. As shown in **Figure 2a**, $PtSe_2$ samples with thickness from 2.2 nm to 7.8 nm show broadband light absorption from 450 nm to over 3000 nm. The absorption peaks have significant red-shift with the increase

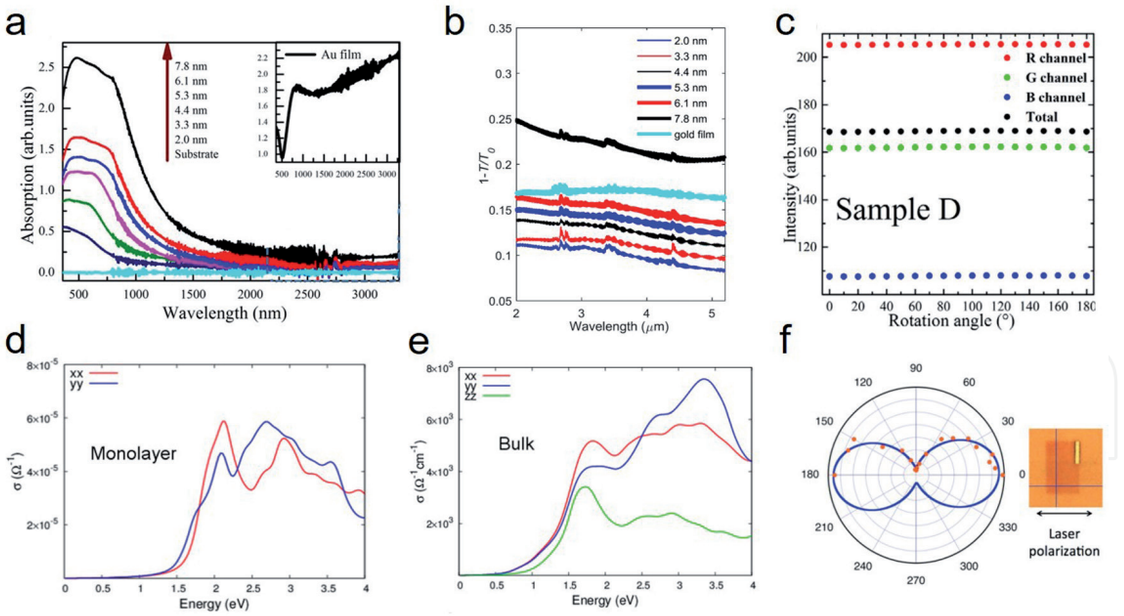

Figure 2.
Optical properties of NTMDs. (a)-(b) Vis-near-IR and mid-IR absorption spectra of $PtSe_2$ with different thickness. The substrates are sapphires and the (a) inset is optical absorption spectrum of 5 nm thick Au film as reference. (c) Reflective intensity of RGB channels as the function of rotational incident angle, which reflect the in-plane isotropic absorption of $PtSe_2$. (a)-(c) are reproduced with permission [35]. (d)and (e) calculated optical conductivity spectra of 1 L and bulk $PdSe_2$, reproduced with permission [33]. (f) Integrated SHG intensity diagram with different rotation angle of line-polarized laser, reproduced with permission [34].

of thickness, which is originates from the narrower energy gap in thicker samples. In particular, the semi-metal nature in thick $PtSe_2$ samples allows them absorb mid-NIR and even far-NIR light. In **Figure 2b**, all of these samples have broadband absorption in the range from 2 to 5 μm, which is different from tradition TMDs materials. The optical polarization properties of $PtSe_2$ were studied by polarized light imaging experiments. The optical responses of 2D $PtSe_2$ film almost unchanged under the incident channel with different rotation angle, which indicate the in-plane isotropic absorption of $PtSe_2$ (**Figure 2c**).

On contrary, due to the unique orthorhombic pentagonal structure, $PdSe_2$ shows anisotropic optical response in the van der Waals plane [33]. From the calculated optical conductivity spectra in **Figure 2d** and **e**, the cut-off energy in bulk $PdSe_2$ is lower than that in 1 L $PdSe_2$, and the conductivity curves in xx and yy direction in both bulk and 2D $PdSe_2$ perform very different characteristics. The anisotropic phenomenon appears at ~1.5 and 1.25 eV in bulk and 2D structure, respectively. The large anisotropy also be predicted at ~2 eV in monolayer $PdSe_2$. Second harmonic generation (SHG) polarization diagram is also performed for observing the anisotropic properties [34]. When the polarization direction of incident light and the crystal orientation are parallel (position of 0° and 180° in **Figure 2f**), the intensity achieves the maximum, while at the position of 0° and 180°, the SHG signal shows significantly decrease.

4. Synthesize of 2D NTMDs

In order to realizing the practical applications of the new kind of TMDs materials, the effective synthesis methods are essential to prepare particular samples with high crystallinity quality, desirable thickness and large lateral size. Up to now, various of synthesis strategies have been conducted to a variety of high-quality NTMDs. Here we do a general review on the different fabrication methods for NTMDs. Chemical vapor transport (CVT) and chemical vapor deposition (CVD) techniques

are most two important methods for NTMDs which are applied to the following photodetector applications.

CVT method is a traditional crystal growth method, which is recently reintroduced for the direct synthesis of TMDs with high crystal quality [36–38]. The synthesis setup is as shown in **Figure 3a** [39]. Pt and Se powders with strict ratio are loaded in the quartz ampoule. After the vapor reactions with the help of a gaseous reactant under high temperature and vacuum, $PtSe_2$ crystals are formed and deposited elsewhere. By carefully adjusting the amounts of reactants and transport, Hu et al. successfully obtained triangular-shaped $PtSe_2$ flakes with 10–50 μm and good controllability [40]. From **Figure 3d**, the optical images exhibit that $PtSe_2$ nanoflakes have controlled layer numbers from 1-layer (1 L) to 20 layers (~20 L) and the atomic force microscope (AFM) images in insets provide the thickness information. The as-grown nanoplates with monocrystalline structure, controllable thickness and large lateral size are very suitable for electronic and photonic devices. Due to the ease of growing bulk crystals by CVT, people also use this method to grow high quality single-crystalline bulk NTMDs and obtain one- to few-layer 2D flakes by peeled from the bulk NTMDs crystal.

CVD is a very common synthesis method in which a large number of 2D materials with scalable size, controllable thickness and high-quality crystal structure have been prepared such as graphene, TMDs, Xene, MXene, boron nitride and so on [41–43]. Recently, the CVD method also be adopted for large-scale NTMDs fabrication. **Figure 3b** shows a CVD selenization method for scalable $PtSe_2$ films. The Pt film as seed were deposited on the substrate (usually the SiO_2 or Si wafer) at first and placed in the center of CVD furnace. The Se powder is at the upstream

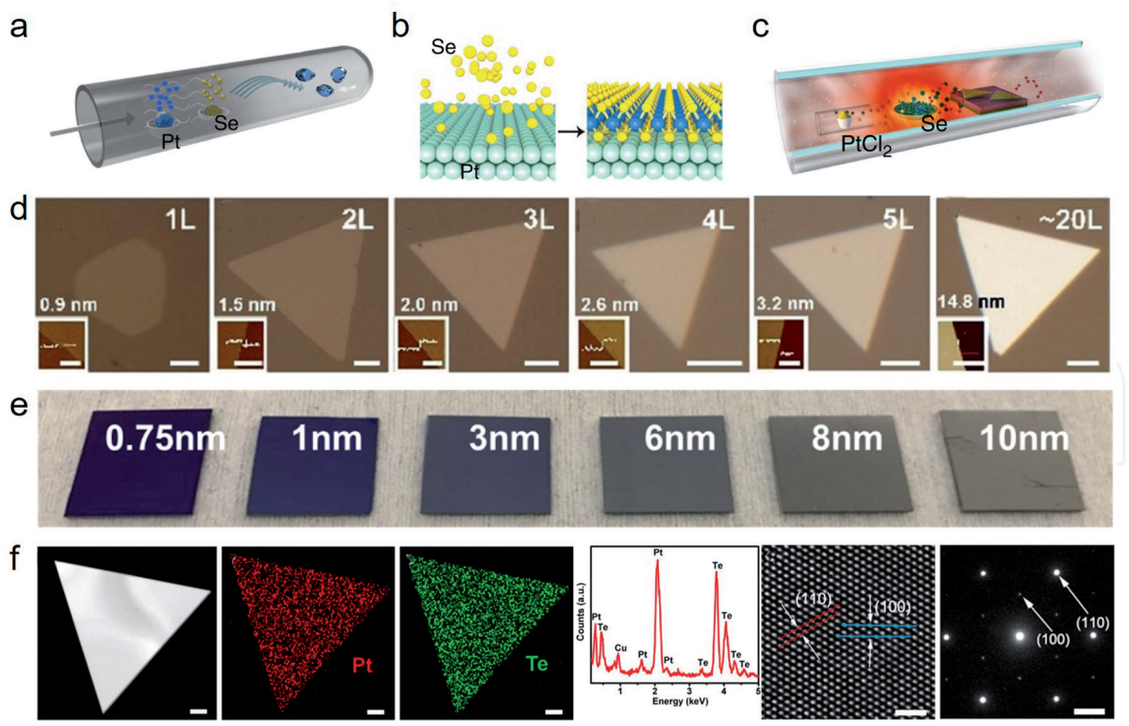

Figure 3.
Materials fabrication for large-scale films and monocrystalline nanosheets. (a) Schematic of CVT method for $PtSe_2$ with controllable thickness, reproduced with permission [39]. (b) Schematic of CVD selenization method for scalable $PtSe_2$ films, reproduced with permission [44]. (c) Schematic of CVD method for the controlled synthesis of NTMDs nanosheets, reproduced with permission [39]. (d) Optical images of PVT-grown $PtSe_2$ flakes with 10–50 μm and controlled layer numbers from 1 L to ~20 L, reproduced with permission [40]. (e) Photographs of CVD-grown 2D $PtSe_2$ polycrystal films from 0.75 to 10 nm, reproduced with permission [45]. (f) Material characterizations for $PtSe_2$ single crystal nanosheets by CVD method, including HAADF-STEM, EDS, Raman, HRTEM and SEAD techniques, reproduced with permission [47].

side. Then the direct selenization of the Pt film happens under high temperature, low pressure and argon gas protection. In 2015, Wang et al. firstly synthesized monolayer $PtSe_2$ nanosheets [44]. Then Han et al. obtained large area $PtSe_2$ film (> a few cm^2) with controllable thickness [45]. **Figure 3e** shows the photographs of as-grown 2D $PtSe_2$ polycrystal films from 0.75 to 10 nm (corresponding to the layer numbers from 1 L to ~15 L). In 2018, Yuan et al. successfully fabricated $PtSe_2$-PtS_2 heterostructure film with wafer-scale and successfully achieved the wafer-scale photodetector application [46]. Besides, CVD method can also synthesize high-quality 2D NTMDs nanocrystals. **Figure 3c** exhibits a schematic of growing 2D nanosheets and through the method, Ma et al. successfully fabricated 2D $PtTe_2$ nanoplates with tunable thickness and a large lateral size up to 80 μm [47]. From **Figure 3f**, the high-angle annular darkfield scanning-TEM (HAADF-STEM) image as well as the EDS mapping analysis shows the well-faceted triangular geometry and the uniformly spatial distribution of Pt and Te elements. The Raman spectrum and High-resolution TEM (HRTEM) furtherly show the high quality of nanosheets and the 6-fold symmetry SEAD pattern shows the hexagonal crystal structure. Type-II Dirac fermions are observed in the high-quality nanocrystal platform. Another advantage of the grown method is that 2D materials can be grown on arbitrary substrates, because both the pre-deposition and post-selenization process do not have strict requirements to the substrate. Till now, 2D NTMDs have been fabricated on different substrates including Si, SiO_2, Sapphire, gallium nitride (GaN), fused quartz, and flexible polyimide.

There are some other synthesize ways for atomic TMDs. Mechanical exfoliation (ME) is one of the most extensively adopted approaches for 2D nanoflakes from their bulk counterparts [13]. Therefore, the as-prepared 2D flakes can maintain the intrinsic structure. Nowadays, most of mechanically exfoliated NTMDs thin flakes are from bulk crystals grown by CVT [48] and self-flux method [26, 49]. These typical nanosheets show the extraordinary electronic properties, but their small lateral size and uncontrollability during the fabrication process limit their application potential in practical devices. Molecular beam epitaxy (MBE) has also been applied for 2D NTMDs, including $PtSe_2$ [50], $PdTe_2$ [51] and $PdSe_2$ [52], which shows the merits of large-size monocrystalline, and controllable thickness on different substrates. For example, the high-quality $PtSe_2$ atomic film was epitaxial grown on bi-layer graphene/6H-SiC substrate through MBE method [50]. The as-grown film had controllable thickness from single-layer to over 22 layers, which shows extraordinary thickness-dependent electronic properties and tunable bandgaps.

5. 2D NTMDs for photodetection

So far, various NTMDs based photodetectors with diverse constructions and high-performance have been reported [53]. **Table 1** summarizes their characteristic parameters. The strong optical absorption capability and large carrier mobility of NTMDs provide high responsivity (R) and detectivity (D*) for these photodetectors, while the narrow bandgaps of atomic layered PtS_2, $PtSe_2$ and $PdSe_2$ make them inherently suitable for NIR detection. For multi-layer NTMDs (over 5 L for $PtSe_2$), which can be regarded as semimetal materials, they can be combined with other semiconductor materials and construct Schottky heterostructures. By choosing a suitable semiconductor functional layer with a particular bandgap (such as n-Si, III – V, 2D perovskite, 2D MoS_2, and so on), the photodetector can work efficiently at a specifical wavelength. In addition, owing to the majority-carrier-dominant current-flow mechanism, photodetectors based on NTMDs heterostructures have advantages in high-speed applications. Combined with other electronic

Device structure	Material grown methods	R (AW^{-1})	τ_r/τ_f	D^* (Jones)	Measurement conditions	Spectral range	Ref.
Few-layer $PtSe_2$	CVT	0.01	—	—	λ = 500 nm, V_g = −80 V	Visible-NIR	[23]
Bilayer $PtSe_2$	CVT + ME	4.5	1.1/1.2 ms	7×10^8	λ = 10 μm, V_b = 0.1 V	Visible-MIR	[39]
Few-layer PtS_2	CVT	1.56×10^3	460/460 ms	2.9×10^{11}	λ = 500 nm, V_b = 0.1 V	Visible	[48]
Few-layer $PdSe_2$	ME	708	—	1.31×10^9	λ = 1064 nm, V_g = 30 V	Visible-MIR	[54]
$PtSe_2$/Si	TAC	0.52	55.3/170.5 μs	3.26×10^{13}	λ = 808 nm, V_b = 0 V	Visible-NIR	[55]
$PtSe_2$/n-Si	TAC	0.49	—	—	λ = 808 nm, V_b = −2 V	UV–NIR	[56]
$PtSe_2$/Ge	CVD	0.602	7.42/16.71 μs	6.31×10^{11}	λ = 1550 nm, V_b = 0 V	Visible-NIR	[59]
$PtSe_2$GaAs	CVD	0.262	5.5/6.5 μs	$\sim 10^2$	λ = 808 nm, V_b = 0 V	DUV–NIR	[60]
$PtSe_2$/GaN	CVD	0.193	45/102 μ	3.8×10^{14}	λ = 265 nm, V_b = 0 V	DUV	[61]
$PtSe_2$/CdTe	CVD	0.51	8.1/43 μs	4.2×10^{11}	λ = 780 nm, V_b = 0 V	DUV–NIR	[62]
$PtSe_2/FA_{0.85}Cs_{0.15}PbI_3$	CVD	0.118	78/60 ns	2.9×10^{12}	λ = 808 nm, V_b = 0 V	UV–NIR	[63]
$PtS_2/PtSe_2$	CVD	0.361	66/75 ms	—	λ = 532 nm, V_b = 0 V	Visible-NIR	[46]
$PdSe_2$/n-Si	CVD	0.3	—	$\sim 10^{13}$	λ = 780 nm, V_b = 0 V	UV–NIR	[57]
G/$PdSe_2$/Ge	CVD	0.69	6.4/92.5 μs	1.73×10^{13}	λ = 265 nm, V_b = 0 V	DUV-MIR	[58]
$PdSe_2/FA_{0.85}Cs_{0.15}PbI_3$	CVD	0.313	3.5/4 μs	$\sim 10^{13}$	λ = 265 nm, V_b = 0 V	DUV-NIR	[64]
$PdSe_2/MoS_2$	CVT	42.1	—	8.21×10^9	λ = 10.6 μm, V_b = 1 V	Visible-MIR	[65]

**The detectivity D of a photodetector is a figure of merit, defined as the inverse of the noise-equivalent power (NEP). The larger the detectivity of a photodetector, the more it is suitable for detecting week signals which compete with the detector noise. But the specific detectivity D* is the detectivity normalized to a unit detector area and detection bandwidth; one can calculate it by multiplying the detectivity with the square root of the product of detector area (in square centimeters) and the detector bandwidth (in Hz). That term is useful for comparing the performance of different detector technologies.*

Table 1.
Summary of characteristic parameters for NTMDs based photodetectors.

characteristics, different photodetectors with wide-spectral, fast-speed, self-powered and anisotropic have been realized. NTMDs based wafer-scalable and flexible photodetectors arrays could be the future development trend. We will comprehensively discuss them in this section.

5.1 2D NTMDs photodetectors

Due to the great electronic transport and optical properties of NTMDs, various of NTMDs based phototransistors have been studied [23, 39, 48, 54]. Here we illustrate a typical PtS_2 phototransistor as an instance [48]. The device schematic is as shown in **Figure 4a**, in which few-layer PtS_2 as the channel material on h-BN substrate. The device shows a high field-effect mobility of ~13 $cm^2V^{-1}S^{-1}$ and the high on/off ratio of 10^5. Then the photo-response ability under light illumination at visible wavelength (500 nm) is studied. Both photogenerated conductive and photo-gating effects are observed in the device. **Figure 4b** is the 3D diagram which shows the combined photocurrent with incident light intensity and gate voltage (V_g). By calculation, the detectivity and responsivity are obtained with the function of V_g (**Figure 4c**). when V_g is zero, the responsivity is highly at 1560 AW^{-1}, which shows 10^6 times higher than that of graphene and 10^3 times higher than that of BP detectors (~0.5 and 657 mAW^{-1}, respectively). Similarly, the detectivity (D*), as the inverse of the noise-equivalent power and the key parameter related to the signal-to-noise rate of the device, reaches 2.9 × 10^{11} Jones, which is also higher than that of other 2D-based devices (**Figure 4c**). The photo-gain is about 2 × 10^6 at 30 V of V_g, which could be the highest gain in 2D-based photodetectors. The few-Layered PtS_2 phototransistor shows that NTMDs is outstanding candidate in photodetection area at visible wavelength range.

Mid-IR optoelectronics is fantastic and important because there is an optical transparent window at Mid-IR in the atmosphere. However, in traditional TMDs

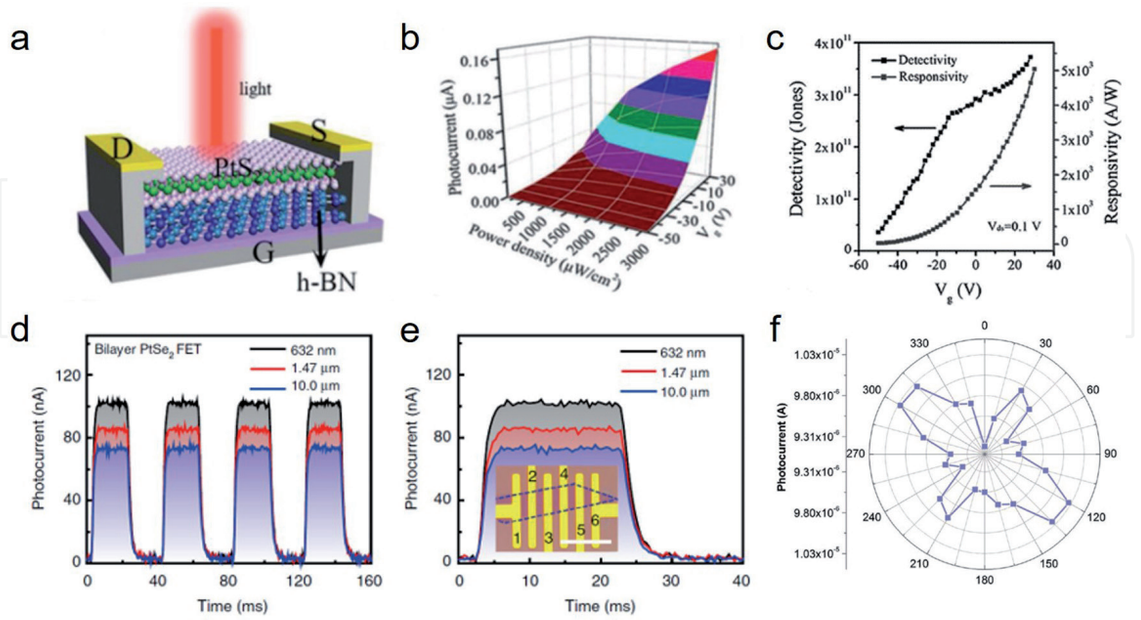

Figure 4.
2D NTMDs phototransistors. (a)-(c) PtS_2 on h-BN for photodetection. (a) Schematic of the device structure. (b) 3D view of photocurrent mapping. (c) the responsivity and detectivity as a function of vg measured at V_{ds} = 0.1 V. (a)-(c) are reproduced with permission [48]. (d)-(f) bilayer $PtSe_2$ for ultrawide spectra photodetection. (d) and (e) time-resolved photo-response curve at the wavelength of 0.63, 1.47 and 10 μm. (d)-(e) are reproduced with permission [39]. (f) Polarized plot diagram which shows the photocurrent of the device as a function of linear polarization rotation. The gate bias is 50 V and the wavelength is 532 nm, reproduced with permission [54].

based photodetectors, it is very difficult to realize the effective detection at Mid-IR. NTMDs can overcome the difficulty due to the narrow bandgap. Yu et al. fabricated a bi-layer $PtSe_2$ based phototransistor, which can realize wide-spectral and sensitive detection from 632 nm to 10 μm [39]. As shown in **Figure 4d** and **e**, the time-resolved photo-response results are obtained at 632 nm, 1.47 μm and 10 μm, with photo-responsivity of 6.25 AW^{-1}, 5.5 AW^{-1} and 4.5 AW^{-1}, respectively. The achieved photo-current responsivity at 10 μm is 3 orders of magnitude higher than that of graphene and comparable to commercial mid-IR detectors. The rise and fall time are also better than other TMDs based photodetectors owing to the high mobility of $PtSe_2$. Overall, bilayer $PtSe_2$ shows promising potential in mid-IR optoelectronic applications.

For anisotropic detector applications, Liang et al. adopted $PdSe_2$ as the photo-sensitive material [54]. The photodetector shows effective photo-response covering from 532 nm to 4.05 μm. The responsivity is 708 AW^{-1}, which is five orders larger than graphene and two orders larger than commercial InGaAs near-IR photodetectors. Furthermore, with the unique pentagonal structure of $PdSe_2$, the detector shows anisotropic photo-response for the linear-polarized light with varying polarization angle. In **Figure 4f**, when the increase of rotation angle with the step of 15° from 0° to 360°, the photocurrent clearly shows periodical variation and reaches the maximum value at 120° and 300°, which is coincident with the angle-resolved polarized Raman response results, furtherly showing the lattice effects. The anisotropic detectors as linear dichroism media have potential in optical communication and structural chemistry analysis.

Overall, with the first realization of $PtSe_2$ photodetectors in 2016 [23], Various of NTMDs and their photodetection abilities are studied, which show great performance. Till now, NTMDs based photodetectors exhibit higher responsivity and photo-gain than that of graphene, conventional TMDs and other 2D photodetectors. The work wavelength has been extended to 10 μm and the anisotropic detection has also been realized. With the development of NTMDs synthesis technique, the optimization of device structure, and the study of NTMDs photo-current mechanism, the narrow bandgap material will be the excellent candidate in the field of photodetection.

5.2 2D NTMDs heterostructures for photodetection

NTMDs with widely tunable energy gaps and high carrier mobility have broad prospects in developing high-performance photodetectors. However, the ultrathin thickness nature makes 2D NTMDs relatively low light absorption. Constructing NTMDs based heterostructures can not only enhance the light absorption, but accelerate the separation and transmission of carriers, and invent the high-speed photodetectors. Therefore, different NTMDs heterostructures have been studied for fast, broadband, self-powered and polarization-sensitive photodetectors.

Due to the atomic thickness, NTMDs is very convenient to from heterostructures with conventional semiconductors such as Si [55], n-Si [56, 57], Ge [58, 59], GaAs [60], GaN [61] and CdTe [62]. Few-layer $PtSe_2$ is semimetal state. By choosing p-doped bulk semiconductors with appropriate work function and bandgaps and contacting them with Few-layer $PtSe_2$ layer, the Schottky junction will be formed. The detection wavelength is determined by the bulk semiconductor. Zeng et al. fabricated the $PtSe_2$-GaAs vertical heterostructure detector [60]. The device schematic and the photocurrent generation mechanism are depicted in **Figure 5a**. Under the light illumination, the electron–hole pairs forms at the interface of the heterojunction, then separates with the function of in-built electric field. The photocurrent generates and gathered by two electrodes. The device shows the broadband work wavelength from200 to 1200 nm and a large photo-response at visible wavelength

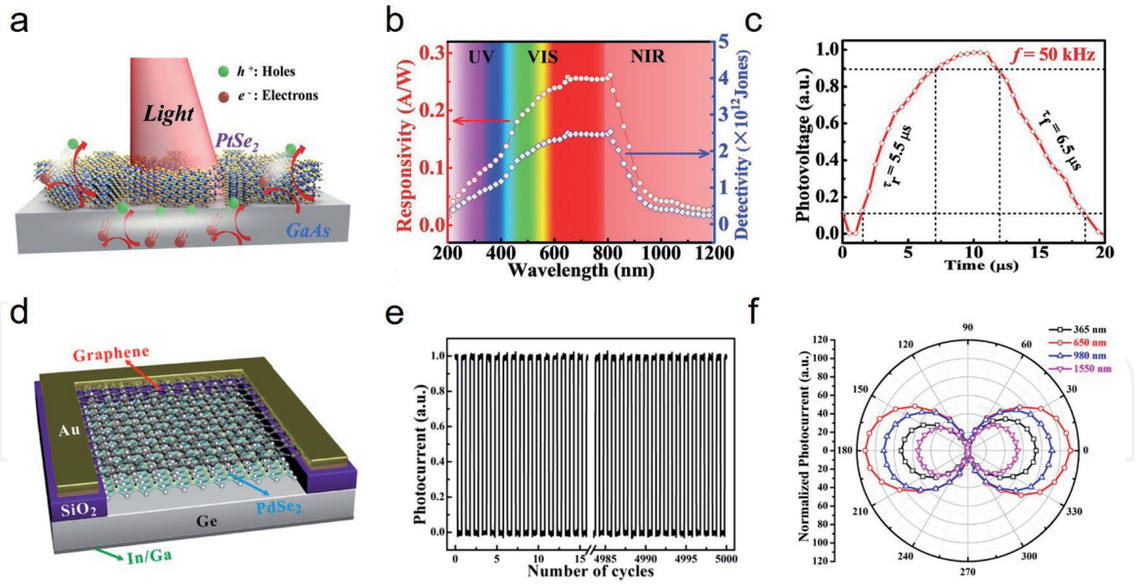

Figure 5.
(a) Device schematic and the photocurrent generation mechanism of the $PtSe_2$-GaAs photodetector. (b) Wavelength-dependent specific detectivity and responsivity of $PtSe_2$-GaAs photodetector. (c) Fast photo-response with the rise/fall time of 5.5/6.5 μs. (a)-(c) are reproduced with permission [60]. (d) Schematic diagram of graphene-$PdSe_2$-Ge based photodetectors. (e) the long-term stability measurement results, where the device still remains stable with continuedly working over 5000 cycles. (f) Normalized photocurrent graphs which obtained by changing illumination polarization angle of linearly polarized light with wavelengths of 365, 650, 980 and 1550 nm. (d)-(f) are reproduced with permission [58].

(**Figure 5b**). The responsivity and specific detectivity reach to 708 mAW^{-1} and 2.9×10^{12} Jones at 808 nm, respectively. Moreover, the device achieves the fast response speed, in which the rise and fall time are only 5.5 and 6.5 μs (**Figure 5c**). By choosing the semiconductor layer with relatively large energy gap, *e.g.,* GaN, the deep-UV photodetectors can be realized [61]. The self-powered $PtSe_2$-GaN phototransistor has the responsivity of 193 mAW^{-1}, an ultra-high specific detectivity of 3.8×10^{14} Jones and a fast response time of 45.2/102.3 μs at zero gate voltage. In particular, the calculated linear dynamic range (LDR) exceeds 155 dB, which much higher than all reported 2D based detectors and commercial photodetectors. For infra-wavelength application, Wang et al. designed a near-infrared light photovoltaic detector by constructing few-layer $PtSe_2$-Ge heterostructure [59]. Since the device works at photovoltaic region, the self-start operation can be realized without any external power supply. The device also has high responsivity (602 mAW^{-1} at 1550 nm, closed to that of commercial device) and long environment stability. Then Wu and the co-workers designed the improved graphene-$PdSe_2$-Ge heterostructure (**Figure 5d**) [58]. With graphene as a transport and protector layer, the device has great stability and can realize the imaging application. In particular, with continuedly working over 5000 cycles, the photo-response still remains stable, showing the practical application potential (**Figure 5e**). Due to the particularity of $PdSe_2$, the device can achieve the dipole anisotropic operation (see **Figure 5f**).

Perovskite is also an emerging material with a large absorption coefficient, long diffusion length and low trapping density, which has aroused extensive research interest in optoelectronics. Zhang et al. reported a new type of detector based on few-layer $PtSe_2$ and $FACsPbI_3$ perovskite heterostructure [63]. The device has broad spectra response from 300 to 1200 nm, with the responsivity of 117.7 mAW^{-1}, high I_{light}/I_{dark} ratio of 5.7×10^3 and considerable specific detectivity of 2.6×10^{12} Jones. Especially, due to the extraordinary electronic properties of $PtSe_2$ and the perovskite and the well-designed built-in electric field at Schottky junction interface, the response time is only 78/60 ns, which is one of the fastest reported values

in mixed-dimensional 2D-3D van der Waals heterostructures. Zeng and the co-workers chose $PtSe_2$ to construct heterojunction with $FA_{1-x}Cs_xPbI_3$ perovskite film, which can realize the self-powered detection operation from 200 to 1550 nm [64]. The device demonstrates high responsivity, large on/off ratio, a good polarization sensitivity over 10^4, and reliable imaging application at 808 nm.

The heterostructure between NTMDs with other 2D materials is also fantastic. Here we use $PdSe_2$-MoS_2 heterostructure as an example [65]. Both of $PdSe_2$ and MoS_2 are multilayer flakes with thickness of ~10 nm. The ultra-thin device can not only a ultrawide spectra working range from 532 nm to 10.6 μm, but contributes an ultrahigh responsivity of 42.1 AW^{-1} at 10.6 μm.

5.3 Perspective of 2D NTMDs in photodetectors

Due to the industrial demand and the inherent advantages of 2D materials, the development trend of 2D optoelectronics is scalability and flexibility. Yuan et al. has realized the fabrication of wafer-scale PtS_2- $PtSe_2$ heterojunctions and devices [46]. They pre-deposited 0.8 nm Pt films as arrays of periodic square, then directly grew PtS_2 and $PtSe_2$ 2D thin films by CVD method. **Figure 6a** is the photograph and **Figure 6b** shows the schematic illustration of one single device. The photodetector array can work from 405 nm to 2200 nm. The ultrathin device has a large external quantum efficiency (EQE) (1.2% at 1064 nm, 0.2% at 1550 nm, and 0.05% at 2200 nm). The response time is several milliseconds. If the quality of thin film is improved, the response time could be faster. The scalable devices can be adopted for high-resolution imaging, as shown in **Figure 6c**.

For the study of NTMDs flexible devices, Su and the co-workers did the pioneer work [66]. $PtSe_2$ thin films with 2.5 nm thickness (~3 L) on flexible polyimide substrate were directly grown by plasma-assisted selenization process, which show p-doped semiconductor behaviors and the average field effect mobility of

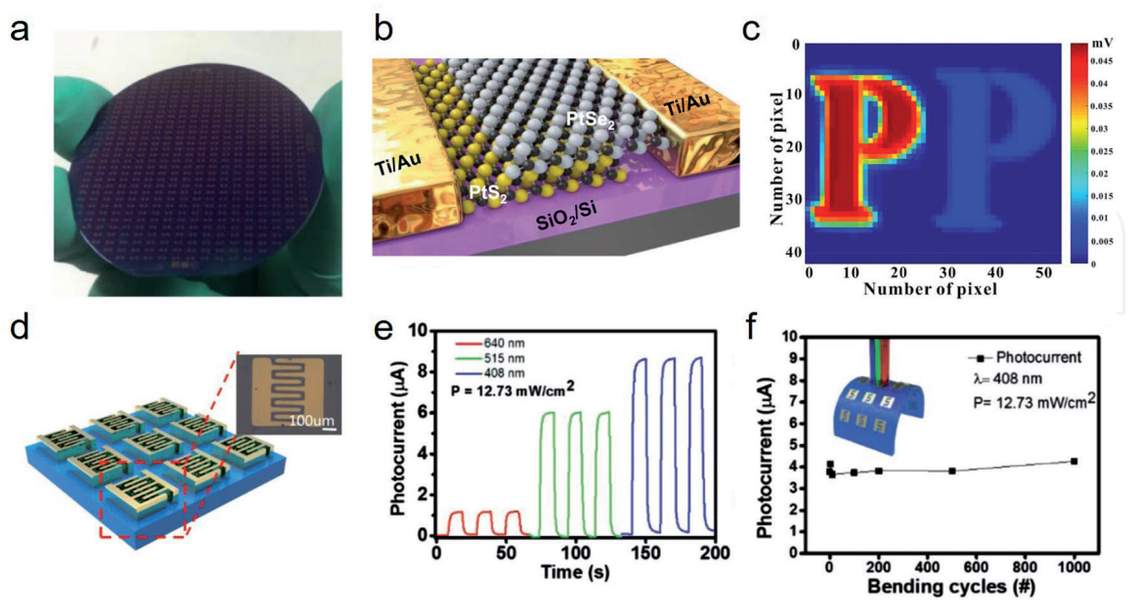

Figure 6.
(a)-(c) Wafer-scale NTMDs photodetection and imaging. (a) Photograph of PtS_2- $PtSe_2$ photodetectors array on a SiO_2/Si wafer. (b) Schematic illustration of the photodetector device. (a)-(b) are reproduced with permission [46]. (c) high-resolution imaging by NTMDs based photodetectors, reproduced with permission [58]. (d)-(f) Flexible photodetection based on $PtSe_2$. (d) illustration of the $PtSe_2$ thin film based Flexible photodetector. (e)Time-resolved photo-response curve at the wavelength of 408, 515 and 640 nm. (f) Mechanic stability measurement, in which the photocurrent is recorded as a function of bending cycles. (e)-(f) are reproduced with permission [66].

0.7 $cm^2V^{-1}S^{-1}$. **Figure 6d** shows the array of devices with the finger-type electrode structure. The flexible photodetector shows good photoresponse with responsivity of 0.4, 0.25 and 0.1AW^{-1} at 408, 515 and 640 nm, respectively (**Figure 6e**). Moreover, the great mechanic stability is exhibited. Under large bending with different radius over 1000 cycles, the device can still generate stable photocurrent with almost no degradation, which is depicted in **Figure 6f**.

6. Conclusions

In this chapter, we focus on 2D NTMDs and their applications in the field of photodetectors. 2D NTMDs exhibit extraordinary structural, electronic and optical properties. Unlike conventional TMD materials, the emerging NTMDs with abundant d-electrons and strong interlayer electronic hybridization have broadband optical absorption and ultra-high mobility, which are promising in optoelectronics. Then we have discussed efficient and controllable synthesis methods for 2D NTMDs with high crystal quality and large scalability. Various NTMDs based photodetectors have been developed till now. We have witnessed their outstanding performance, including wide-spectral range, ultrafast response, self-power and anisotropy. With the development of the materials technology and device manufacturing technology, NTMDs will have great potential in practical optoelectronic applications.

Acknowledgements

This work is supported by the Starting Research Funds from Songshan Lake Materials Laboratory, China (No. Y0D1051F211). Dr. Jian yuan acknowledges the support from Natural Science Research Project for Anhui Universities (grant no. KJ2019A0596), and Youth Project of Provincial Natural Science Foundation of Anhui (grant no. 2008085QF319).

Conflict of interest

The authors declare no conflict of interest.

DOI: http://dx.doi.org/10.5772/intechopen.95883

Author details

Haoran Mu[1,2], Jian Yuan[3] and Shenghuang Lin[1*]

1 Songshan Lake Materials Laboratory, Dongguan, China

2 Department of Materials Science and Engineering and ARC Centre of Excellence in Future Low-Energy Electronics Technologies (FLEET), Monash University, Clayton, Victoria, Australia

3 School of Physics and Electronic Information, Huaibei Normal University Huaibei, Anhui, P.R. China

*Address all correspondence to: linshenghuang@sslab.org.cn

References

[1] Arquer FPG, Armin A, Meredith P, Sargent EH. Solution-processed semiconductors for next-generation photodetectors. Nature Reviews Materials. 2017;2(3): 1-17.

[2] Donati S. Photodetectors: Prentice Hall PTR; 1999.

[3] Zhai T, Fang X, Liao M, Xu X, Zeng H, Yoshio B, et al. A comprehensive review of one-dimensional metal-oxide nanostructure photodetectors. Sensors. 2009;9(8):6504-29.

[4] Sang L, Liao M, Sumiya M. A comprehensive review of semiconductor ultraviolet photodetectors: from thin film to one-dimensional nanostructures. Sensors. 2013;13(8):10482-518.

[5] Zhong Y, Malagari SD, Hamilton T, Wasserman DM. Review of mid-infrared plasmonic materials. Journal of Nanophotonics. 2015;9(1):093791.

[6] Champness NR. Two-dimensional materials: Crystallized creations in 2D. Nature Chemistry. 2014;6(9):757-9.

[7] Xia F, Wang H, Xiao D, Dubey M, Ramasubramaniam A. Two-dimensional material nanophotonics. Nature Photonics. 2014;8(12):899-907.

[8] Burch KS, Mandrus D, Park J-G. Magnetism in two-dimensional van der Waals materials. Nature. 2018;563(7729):47-52.

[9] Low T, Chaves A, Caldwell JD, Kumar A, Fang NX, Avouris P, et al. Polaritons in layered two-dimensional materials. Nature Materials. 2017;16(2):182-94.

[10] Ferrari AC, Bonaccorso F, Fal'Ko V, Novoselov KS, Roche S, Boggild P, et al. Science and technology roadmap for graphene, related two-dimensional crystals, and hybrid systems. Nanoscale. 2015;7(11):4598-810.

[11] Ponraj JS, Xu Z-Q, Dhanabalan SC, Mu H, Wang Y, Yuan J, et al. Photonics and optoelectronics of two-dimensional materials beyond graphene. Nanotechnology. 2016;27(46):462001.

[12] Tan C, Cao X, Wu X-J, He Q, Yang J, Zhang X, et al. Recent advances in ultrathin two-dimensional nanomaterials. Chemical Reviews. 2017;117(9):6225-331.

[13] Wang QH, Kalantar-Zadeh K, Kis A, Coleman JN, Strano MS. Electronics and optoelectronics of two-dimensional transition metal dichalcogenides. Nature Nanotechnology. 2012;7(11):699-712.

[14] Hu Z, Wu Z, Han C, He J, Ni Z, Chen W. Two-dimensional transition metal dichalcogenides: interface and defect engineering. Chemical Society Reviews. 2018;47(9):3100-28.

[15] Choi W, Choudhary N, Han GH, Park J, Akinwande D, Lee YH. Recent development of two-dimensional transition metal dichalcogenides and their applications. Materials Today. 2017;20(3):116-30.

[16] Jariwala D, Sangwan VK, Lauhon LJ, Marks TJ, Hersam MC. Emerging device applications for semiconducting two-dimensional transition metal dichalcogenides. ACS Nano. 2014;8(2):1102-20.

[17] Tian X, Kim DS, Yang S, Ciccarino CJ, Gong Y, Yang Y, et al. Correlating the three-dimensional atomic defects and electronic properties of two-dimensional transition metal dichalcogenides. Nature Materials. 2020:1-7.

[18] Pi L, Li L, Liu K, Zhang Q, Li H, Zhai T. Recent Progress

on 2D Noble-Transition-Metal Dichalcogenides. Advanced Functional Materials. 2019;29(51):1904932.

[19] Chen E, Xu W, Chen J, Warner J. 2D layered noble metal dichalcogenides (Pt, Pd, Se, S) for electronics and energy applications. Materials Today Advances. 2020;7:100076.

[20] Gong Y, Lin Z, Chen Y-X, Khan Q, Wang C, Zhang B, et al. Two-Dimensional Platinum Diselenide: Synthesis, Emerging Applications, and Future Challenges. Nano-Micro Letters. 2020;12(1):1-34.

[21] Zhao Y, Qiao J, Yu P, Hu Z, Lin Z, Lau SP, et al. Extraordinarily strong interlayer interaction in 2D layered PtS_2. Advanced Materials. 2016;28(12):2399-407.

[22] Yang H, Kim SW, Chhowalla M, Lee YH. Structural and quantum-state phase transitions in van der Waals layered materials. Nature Physics. 2017;13(10):931-7.

[23] Zhao Y, Qiao J, Yu Z, Yu P, Xu K, Lau SP, et al. High-electron-mobility and air-stable 2D layered $PtSe_2$ FETs. Advanced Materials. 2017;29(5):1604230.

[24] Wang Z, Li Q, Besenbacher F, Dong M. Facile synthesis of single crystal $PtSe_2$ nanosheets for nanoscale electronics. Advanced Materials. 2016;28(46):10224-9.

[25] Li G, Zhang Y-Y, Guo H, Huang L, Lu H, Lin X, et al. Epitaxial growth and physical properties of 2D materials beyond graphene: from monatomic materials to binary compounds. Chemical Society Reviews. 2018;47(16):6073-100.

[26] Oyedele AD, Yang S, Liang L, Puretzky AA, Wang K, Zhang J, et al. $PdSe_2$: pentagonal two-dimensional layers with high air stability for electronics. Journal of the American Chemical Society. 2017;139(40):14090-7.

[27] Wang Y, Li Y, Chen Z. Not your familiar two dimensional transition metal disulfide: structural and electronic properties of the PdS_2 monolayer. Journal of Materials Chemistry C. 2015;3(37):9603-8.

[28] Chow WL, Yu P, Liu F, Hong J, Wang X, Zeng Q, et al. High mobility 2D palladium diselenide field-effect transistors with tunable ambipolar characteristics. Advanced Materials. 2017;29(21):1602969.

[29] Chhowalla M, Shin HS, Eda G, Li L-J, Loh KP, Zhang H. The chemistry of two-dimensional layered transition metal dichalcogenide nanosheets. Nature Chemistry. 2013;5(4):263-75.

[30] Kappera R, Voiry D, Yalcin SE, Branch B, Gupta G, Mohite AD, et al. Phase-engineered low-resistance contacts for ultrathin MoS_2 transistors. Nature Materials. 2014;13(12):1128-34.

[31] Huang H, Fan X, Singh DJ, Zheng W. Modulation of Hydrogen Evolution Catalytic Activity of Basal Plane in Monolayer Platinum and Palladium Dichalcogenides. ACS Omega. 2018;3(8):10058-65.

[32] Setiyawati I, Chiang K-R, Ho H-M, Tang Y-H. Distinct electronic and transport properties between 1T-$HfSe_2$ and 1T-$PtSe_2$. Chinese Journal of Physics. 2019;62:151-60.

[33] Sun J, Shi H, Siegrist T, Singh DJ. Electronic, transport, and optical properties of bulk and mono-layer $PdSe_2$. Applied Physics Letters. 2015;107(15):153902.

[34] Puretzky AA, Oyedele AD, Xiao K, Haglund AV, Sumpter BG, Mandrus D, et al. Anomalous interlayer vibrations in strongly coupled layered $PdSe_2$. 2D Materials. 2018;5(3):035016.

[35] Xie J, Zhang D, Yan X-Q, Ren M, Zhao X, Liu F, et al. Optical properties of chemical vapor deposition-grown $PtSe_2$ characterized by spectroscopic ellipsometry. 2D Materials. 2019;6(3):035011.

[36] Hu D, Xu G, Xing L, Yan X, Wang J, Zheng J, et al. Two-dimensional semiconductors grown by chemical vapor transport. Angewandte Chemie International Edition. 2017;56(13):3611-5.

[37] Wang J, Zheng H, Xu G, Sun L, Hu D, Lu Z, et al. Controlled Synthesis of Two-Dimensional 1T-$TiSe_2$ with Charge Density Wave Transition by Chemical Vapor Transport. Journal of the American Chemical Society. 2016;138(50):16216-9.

[38] Du Z, Zhang C, Wang M, Zhang X, Ning J, Lv X, et al. Synthesis of $WS_{1.76}Te_{0.24}$ alloy through chemical vapor transport and its high-performance saturable absorption. Scientific Reports. 2019;9(1):1-9.

[39] Yu X, Yu P, Wu D, Singh B, Zeng Q, Lin H, et al. Atomically thin noble metal dichalcogenide: a broadband mid-infrared semiconductor. Nature Communications. 2018;9(1):1-9.

[40] Hu D, Zhao T, Ping X, Zheng H, Xing L, Liu X, et al. Unveiling the layer-dependent catalytic activity of $PtSe_2$ atomic crystals for the hydrogen evolution reaction. Angewandte Chemie. 2019;131(21):7051-5.

[41] Li X, Cai W, An J, Kim S, Nah J, Yang D, et al. Large-area synthesis of high-quality and uniform graphene films on copper foils. Science. 2009;324(5932):1312-4.

[42] Najmaei S, Liu Z, Zhou W, Zou X, Shi G, Lei S, et al. Vapour phase growth and grain boundary structure of molybdenum disulphide atomic layers. Nature Materials. 2013;12(8):754-9.

[43] Sun J, Lu C, Song Y, Ji Q, Song X, Li Q, et al. Recent progress in the tailored growth of two-dimensional hexagonal boron nitride via chemical vapour deposition. Chemical Society Reviews. 2018;47(12):4242-57.

[44] Wang Y, Li L, Yao W, Song S, Sun J, Pan J, et al. Monolayer $PtSe_2$, a new semiconducting transition-metal-dichalcogenide, epitaxially grown by direct selenization of Pt. Nano letters. 2015;15(6):4013-8.

[45] Han SS, Kim JH, Noh C, Kim JH, Ji E, Kwon J, et al. Horizontal-to-vertical transition of 2D layer orientation in low-temperature chemical vapor deposition-grown $PtSe_2$ and its influences on electrical properties and device applications. ACS Applied Materials & Interfaces. 2019;11(14):13598-607.

[46] Yuan J, Sun T, Hu Z, Yu W, Ma W, Zhang K, et al. Wafer-scale fabrication of two-dimensional PtS_2/$PtSe_2$ heterojunctions for efficient and broad band photodetection. ACS Applied Materials & Interfaces. 2018;10(47):40614-22.

[47] Ma H, Chen P, Li B, Li J, Ai R, Zhang Z, et al. Thickness-tunable synthesis of ultrathin type-II Dirac semimetal $PtTe_2$ single crystals and their thickness-dependent electronic properties. Nano Letters. 2018;18(6):3523-9.

[48] Li L, Wang W, Chai Y, Li H, Tian M, Zhai T. Few-layered PtS_2 phototransistor on h-BN with high gain. Advanced Functional Materials. 2017;27(27):1701011.

[49] Shawkat MS, Chung H-S, Dev D, Das S, Roy T, Jung Y. Two-dimensional/three-dimensional Schottky junction photovoltaic devices realized by the direct CVD growth of vdw 2D $PtSe_2$ layers on silicon. ACS Applied Materials & Interfaces. 2019;11(30):27251-8.

[50] Zhou J, Kong X, Sekhar MC, Lin J, Le Goualher F, Xu R, et al. Epitaxial Synthesis of Monolayer $PtSe_2$ Single Crystal on MoSe2 with Strong Interlayer Coupling. ACS Nano. 2019;13(10):10929-38.

[51] Li E, Zhang R-Z, Li H, Liu C, Li G, Wang J-O, et al. High quality $PdTe_2$ thin films grown by molecular beam epitaxy. Chinese Physics B. 2018;27(8):086804.

[52] Li E, Wang D, Fan P, Zhang R, Zhang Y-Y, Li G, et al. Construction of bilayer $PdSe_2$ on epitaxial graphene. Nano Research. 2018;11(11):5858-65.

[53] Yao J, Yang G. 2D material broadband photodetectors. Nanoscale. 2020;12(2):454-76.

[54] Liang Q, Wang Q, Zhang Q, Wei J, Lim SX, Zhu R, et al. High-Performance, Room Temperature, Ultra-Broadband Photodetectors Based on Air-Stable $PdSe_2$. Advanced Materials. 2019;31(24):1807609.

[55] Xie C, Zeng L, Zhang Z, Tsang Y-H, Luo L, Lee J-H. High-performance broadband heterojunction photodetectors based on multilayered $PtSe_2$ directly grown on a Si substrate. Nanoscale. 2018;10(32):15285-93.

[56] Yim C, McEvoy N, Riazimehr S, Schneider DS, Gity F, Monaghan S, et al. Wide spectral photoresponse of layered platinum diselenide-based photodiodes. Nano Letters. 2018;18(3):1794-800.

[57] Zeng LH, Wu D, Lin SH, Xie C, Yuan HY, Lu W, et al. Controlled synthesis of 2D palladium diselenide for sensitive photodetector applications. Advanced Functional Materials. 2019;29(1):1806878.

[58] Wu D, Guo J, Du J, Xia C, Zeng L, Tian Y, et al. Highly polarization-sensitive, broadband, self-powered photodetector based on graphene/$PdSe_2$/germanium heterojunction. ACS Nano. 2019;13(9):9907-17.

[59] Wang L, Li J-J, Fan Q, Huang Z-F, Lu Y-C, Xie C, et al. A high-performance near-infrared light photovoltaic detector based on a multilayered $PtSe_2$/Ge heterojunction. Journal of Materials Chemistry C. 2019;7(17):5019-27.

[60] Zeng LH, Lin SH, Li ZJ, Zhang ZX, Zhang TF, Xie C, et al. Fast, self-driven, air-Stable, and broadband photodetector based on vertically aligned $PtSe_2$/GaAs heterojunction. Advanced Functional Materials. 2018;28(16):1705970.

[61] Zhuo R, Zeng L, Yuan H, Wu D, Wang Y, Shi Z, et al. In-situ fabrication of $PtSe_2$/GaN heterojunction for self-powered deep ultraviolet photodetector with ultrahigh current on/off ratio and detectivity. Nano Research. 2019;12(1):183-9.

[62] Wu D, Wang Y, Zeng L, Jia C, Wu E, Xu T, et al. Design of 2D layered $PtSe_2$ heterojunction for the high-performance, room-temperature, broadband, infrared photodetector. ACS Photonics. 2018;5(9):3820-7.

[63] Zhang Z-X, Zeng L-H, Tong X-W, Gao Y, Xie C, Tsang YH, et al. Ultrafast, self-driven, and air-stable photodetectors based on multilayer $PtSe_2$/perovskite heterojunctions. The Journal of Physical Chemistry Letters. 2018;9(6):1185-94.

[64] Zeng LH, Chen QM, Zhang ZX, Wu D, Yuan H, Li YY, et al. Multilayered $PdSe_2$/Perovskite Schottky Junction for Fast, Self-Powered, Polarization-Sensitive, Broadband Photodetectors, and Image Sensor Application. Advanced Science. 2019;6(19):1901134.

[65] Long M, Wang Y, Wang P, Zhou X, Xia H, Luo C, et al. Palladium diselenide long-wavelength infrared photodetector with high sensitivity and stability. ACS Nano. 2019;13(2):2511-9.

[66] Su TY, Medina H, Chen YZ, Wang SW, Lee SS, Shih YC, et al. Phase-engineered $PtSe_2$-layered films by a plasma-assisted selenization process toward all $PtSe_2$-based field effect transistor to highly sensitive, flexible, and wide-spectrum photoresponse photodetectors. Small. 2018;14(19):1800032.